

---

**Forschungszentrum Karlsruhe**  
Technik und Umwelt

---

**Wissenschaftliche Berichte**  
FZKA 6260

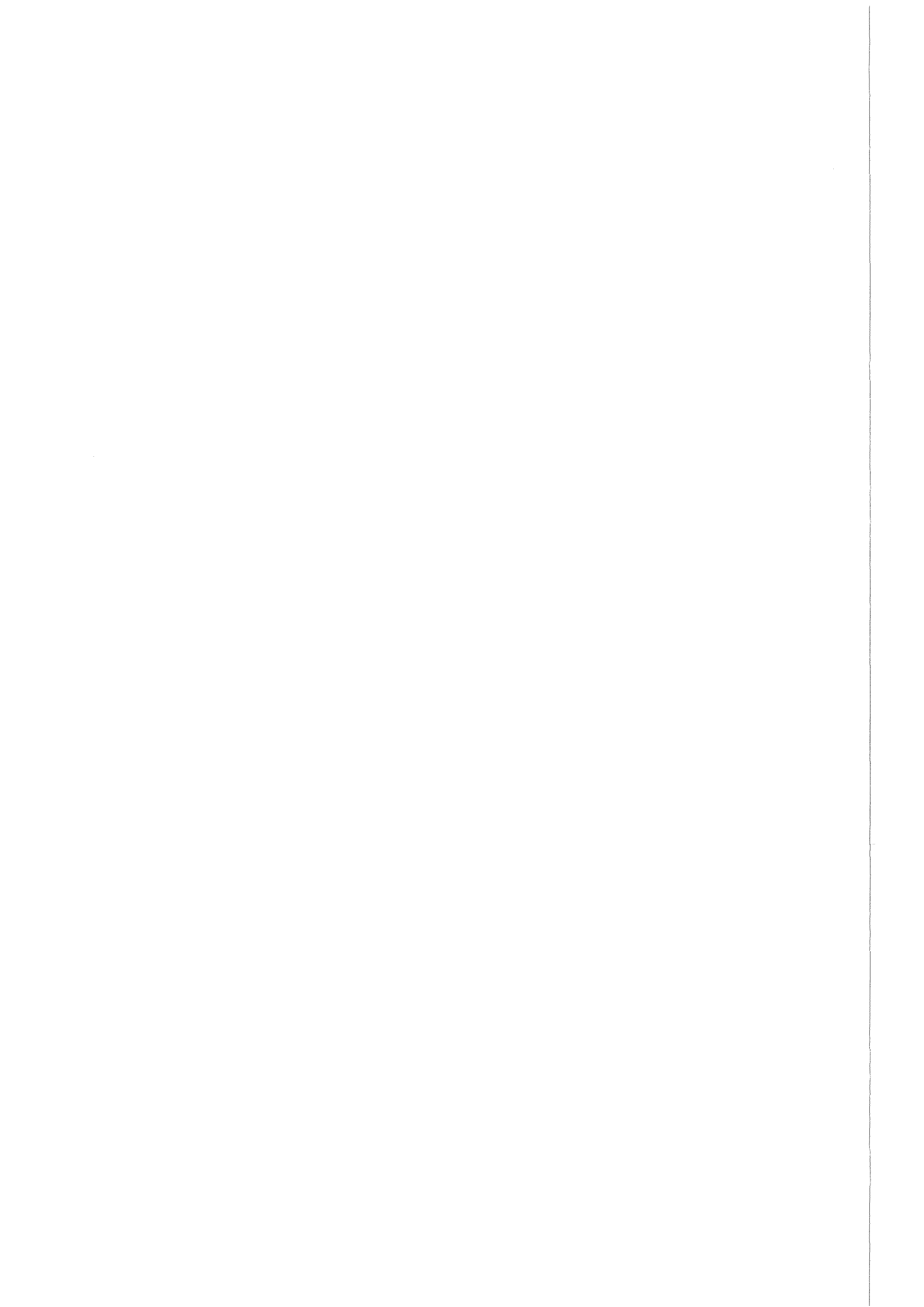
**Similarity solutions,  
KATS experiments and  
CORFLOW results**

**J. J. Foit, A. Vesper**

Institut für Angewandte Thermo- und Fluidodynamik  
Institut für Neutronenphysik und Reaktortechnik  
Projekt Nukleare Sicherheitsforschung

**April 1999**

---



**Forschungszentrum Karlsruhe**

Technik und Umwelt

Wissenschaftliche Berichte

FZKA 6260

**Similarity solutions, KATS experiments  
and CORFLOW results**

**J. J. Foit, A. Vesper**

Institut für Angewandte Thermo- und Fluidodynamik  
Institut für Neutronenphysik und Reaktortechnik

Projekt Nukleare Sicherheitsforschung

Forschungszentrum Karlsruhe GmbH, Karlsruhe  
1999

**Als Manuskript gedruckt**  
**Für diesen Bericht behalten wir uns alle Rechte vor**  
**Forschungszentrum Karlsruhe GmbH**  
**Postfach 3640, 76021 Karlsruhe**  
**Mitglied der Hermann von Helmholtz-Gemeinschaft**  
**Deutscher Forschungszentren (HGF)**  
**ISSN 0947-8620**

## **Similarity solutions, KATS-experiments and CORFLOW results**

### **Abstract**

The current concept of the EPR (European Pressurised Water Reactor) relies on a sufficiently homogeneous spreading of the melt in order to ensure its coolability after a passive initiation of flooding by water. The conditions under which a complete spreading can be expected are the subject of current theoretical and experimental results.

The CORFLOW code allows to treat three-dimensional non-isothermal free surface flow. The influence of cooling on the spreading is modelled by a temperature dependent viscosity. The increase of the viscosity in the thermal boundary layer of the melt can eventually lead to a stop of the melt front. The experimental findings from the KATS series are analysed and CORFLOW results are presented. In addition the available similarity solutions are also used to validate the CORFLOW code.

## **Selbstähnliche Lösungen, KATS-Experimente und CORFLOW Validierung**

### **Zusammenfassung**

Das Konzept des EPR (European Pressurized Water Reactor) basiert auf einer ausreichend homogenen Ausbreitung der Kernschmelze, um deren Kühlung durch ein passiv ausgelöstes Fluten mit Wasser zu gewährleisten. Die Bedingungen, unter denen eine vollständige Ausbreitung zu erwarten ist, sind Gegenstand theoretischer als auch experimenteller Untersuchungen.

Das CORFLOW-Rechenprogramm behandelt dreidimensionale Strömungen mit einer freien Oberfläche. Der Einfluß der Kühlung auf die Ausbreitung wird durch eine temperaturabhängige Viskosität beschrieben. Der Anstieg der Viskosität in der thermischen Grenzschicht, die sich in der Schmelze ausbildet, kann zum Anhalten der Ausbreitungsfront führen. Die experimentellen Ergebnisse der KATS-Experimente werden analysiert und die CORFLOW-Rechenergebnisse dargestellt. Zusätzlich wird CORFLOW anhand von vorhandenen selbstähnlichen Lösungen validiert.

## Contents

1.	Introduction.....	1
2.	Short description of the code.....	2
3.	CORFLOW validation.....	2
4.	Analysis of the oxidic KATS experiments.....	7
4.1	CORFLOW results.....	8
4.1.1	Melt front progression.....	8
4.1.2	Temperature and velocity profiles for KATS5 experiment.....	12
4.1.3	Energy losses.....	14
5.	Conclusions.....	18
	References.....	20

## 1. Introduction

Recently, the spreading under gravity has received much attention in the field of nuclear safety research. In the case of a postulated melt down accident with a failure of the reactor pressure vessel, the ex-vessel melt will first be collected in the reactor cavity until a melt-through of a gate. Afterwards the gate opens, the corium melt is released into a spreading compartment. The current concept of the EPR (European Pressurised Water Reactor) relies on a sufficiently homogeneous spreading of the melt in order to ensure its coolability after a passive initiation of flooding by water. The conditions under which a complete spreading can be expected are the subject of current theoretical and experimental studies. In the framework of large-scale KATS experiments (FZK, Germany) the non-isothermal spreading of metallic and oxidic melts on ceramic or concrete surfaces under various conditions are studied, e. g. melt overheat and melt release rates.

The numerical simulations are performed with the CORFLOW code which was developed at Siemens (Germany). The code allows to treat three-dimensional non-isothermal free surface flows. The experimental findings from the KATS series are analysed and CORFLOW results are presented. In addition the available similarity solutions are also used to validate the CORFLOW code.

In many applications the cooling process will lead to variable flow properties, e. g. variable viscosity and, consequently, to a coupled system of the temperature and flow equations. It is impossible to satisfactorily treat this problem analytically. The lubrication approximation leads to an equation for which similarity solutions for various conditions have been found by many authors [1], [2], [3], [4]. Bercovici [5] developed a model for an axisymmetric gravity current which accounts for thermoviscous effects, i. e., the spatial variation of the viscosity. The numerical results showed significant deviations from the similarity profiles of the constant viscosity [3] as well as the time-dependent viscosity [4] case. A variety of experiments have been carried out to determine the effects of cooling on the flow of fluids with different properties. The influence of the crust formation rates on the fluid flow was explored experimentally by Fink and Griffiths [6] with the aim of understanding and classifying small-scale flow surface morphology for a fluid with weakly temperature dependent viscosity (polyethylene glycol 600). This study indicated that a crust does not greatly affect the fluid flow except for very high crust formation rates. Experiments which used a fluid with strongly temperature dependent viscosity (glucose syrup) were performed by M. V. Stasiuk et al. [7]. In this case the cold, viscous fluid accumulated at the leading edge,

altering the flow shape and thickness and slowing the spreading. The front became steeper and the surface behind the front was nearly horizontal. All performed experiments evolved to a stage at which the overall spreading behaviour of the flow can be approximated by a constant bulk viscosity.

## 2. Short description of the code

The CORFLOW code [8] simulates the free surface flow of an incompressible fluid in a 3-dimensional geometry. In addition to the fluid, several structure materials can be considered as hydrodynamic obstacles or thermodynamic heat sources. The fluid is assumed to possess Newtonian or non-Newtonian rheology. The free surface is determined by an equation which results from the free interface kinematic boundary condition and an integration of the continuity equation in the vertical direction. The free interface is represented as a height function either as a step function or a second-order polynomial. Internal heat transport by conduction and convection as well as heat generation (decay heat) and heat transfer to the surroundings are modelled. The material properties, except the surface tension, may depend on temperature. A discrete phase transition model is available to simulate solidification and melting of the fluid and phase transition of the structure materials. The influence of the solidification process on the spreading is modelled by an increase of the viscosity. The increase of the viscosity in the thermal boundary layer of the melt can eventually lead to a stop of the melt front.

## 3. CORFLOW validation

After the numerical deficiencies in the treatment of non-isothermal flows with increasing viscosity have been eliminated, there is a need for validation of the achieved modifications. For this purpose the self-similar solutions for spreading with variable viscosity [4] will be used. In this section a survey of the results which are necessary to construct appropriate input data for CORFLOW simulations will be given.

Using the lubrication theory the following evolution equation for the fluid shape  $h(x,t)$  holds [9]:

$$\frac{\partial h}{\partial t} - \frac{1}{3} \frac{g}{\nu} \frac{\partial}{\partial x} \left( h^3 \frac{\partial h}{\partial x} \right) = 0 \quad \text{in } \mathbf{R} \times (0, T) \quad (1)$$

where  $\nu$  is the kinematic viscosity and  $g$  the gravity constant. The spreading of a fluid droplet with the shape  $h_0(x)$  and the volume  $\int_{\mathbf{R}} h_0(x) dx$  is described by Eq. (1) and the initial data

$$h(x, 0) = h_0(x). \quad (2)$$

There is a well-established mathematical theory of the problem (1), (2) [10]. One of the most important differences between the solutions of Eq. (1) and the solutions of the linear diffusion equation is the existence of solutions which vanish outside a closed and bounded set. Furthermore, the interface propagates with finite velocity except possibly at  $t = 0$ . The instantaneous release of the volume  $q$  of the fluid is described by the initial data given by

$$h(x, 0) = q\delta(x) \quad (3)$$

where  $\delta(x)$  denotes the Dirac distribution. A self-similar solution of the above problem was obtained by Zel'dovich and Kompaneets [1]. In [11] it was proven that the solution of Eq. (1) with the initial data given by Eq. (2) behaves asymptotically for  $t \rightarrow \infty$  like the similarity solution with initial data (Eq. 3), i. e.

$$h_{h_0}(x, t) \xrightarrow{t \rightarrow \infty} h_\delta(x, t) \quad (4)$$

The above property allows to compare the long-term behaviour of the release of a fixed volume of fluid with predictions of the self-similar solutions. It can be also used for code validation.

Assuming that the viscosity is a function of time of the form

$$\nu = \gamma t^\beta, \quad \gamma = \frac{\nu_0}{t_0^\beta}, \quad \beta \geq 0 \quad (5)$$

where  $\nu_0$  is the initial viscosity of the fluid, self-similar solutions of Eq. (1) with initial data given by Eq. (3) were obtained by Sakimoto, Zuber [2] and Foit [4]. To derive the similarity solution in the axisymmetric geometry, Sakimoto and Zuber [2] used instead the relation (5) the formula  $\nu = \nu_0 t^\beta$  which cannot be correct for dimensional reasons.

The position of the interfaces as a function of time can be written as

$$x_f^\pm = \pm \eta_f \left( \frac{gq^3}{3\gamma} \right)^{1/5} t^{1/5(1-\beta)}, \quad 0 \leq \beta < 1 \quad (6)$$

The constant  $\eta_f$  is given by

$$\eta_f = 2^{-3/5} \left[ \frac{3}{10} (1 - \beta) \right]^{-1/5} \left[ \frac{1}{5} \pi^{1/2} \frac{\Gamma\left(\frac{1}{3}\right)}{\Gamma\left(\frac{5}{6}\right)} \right]^{-3/5} \quad (7)$$

The spreading of a liquid with a volume which increases as a power law in time is described in terms of the following boundary-value problem with a zero initial fluid volume [12], i. e.

$$h(x, 0) = 0, \quad (8)$$

$$-\frac{1}{3} \frac{g}{\gamma} t^{-\beta} h^3 \frac{\partial h}{\partial x} \Big|_{x=0_{\pm}} = f_{\pm}(t) \quad (9)$$

where  $f_{\pm}(t)$  is the mass flux in the positive and negative directions, respectively, and is given by

$$f_{\pm}(t) = \pm \frac{1}{2} \alpha q t^{\alpha-1}, \quad \alpha > 0. \quad (10)$$

The above problem has an exact solution for every value  $\alpha = \frac{4}{3}(1 - \beta)$  with  $0 \leq \beta < 1$ . For other values  $\alpha > 0$  and  $0 \leq \beta < 3\alpha + 1$  approximate similarity solutions are derived in [4], [12].

The positions of the interfaces are defined as follows:

$$x_f^{\pm} = \pm \eta_f \left( \frac{gq^3}{3\gamma} \right)^{1/5} t^{1/5(3\alpha - \beta + 1)} \quad (11)$$

with

$$\eta_f = \left[ \frac{2}{3\alpha} c_1^4 (1 + c_2)^3 (1 - 4c_2) \right]^{-3/5} \quad (12)$$

and

$$c_1 = \left[ \frac{3}{5} (3\alpha - \beta + 1) \right]^{1/3}, \quad (13)$$

$$c_2 = \left[ \frac{3\alpha + 4\beta - 4}{24(3\alpha - \beta + 1)} \right]^{1/3} \quad (14)$$

The presented solutions are expected to be valid only if the viscous forces are much higher than the inertial forces. Using the arguments as in [3] one can show that for flows for which  $4\alpha - 3\beta - 7 < 0$ ,  $\alpha > 0$  the viscous forces are dominant for all  $t \gg t_{ir}$ . In [4] it was shown that if the parameter  $t_0$  in Eq. (5) is chosen to be  $t_0 = \tau_{ir}$ ,

$$\tau_{ir} = \left( \frac{l}{\eta_f^{10} \Big|_{\beta=0}} \frac{q^4}{g^2 v_0^3} \right)^{-\frac{1}{4\alpha-7}} \quad (15)$$

which is the transition time for spreading with constant viscosity ( $\beta = 0$ ) and flow rates determined by  $\alpha$ , the transition time  $t_{ir}$  is given by

$$t_{ir}(\alpha, \beta) = \left( \frac{\eta_f^{10} \Big|_{\beta=0}}{\eta_f^{10}} \right)^{-\frac{1}{4\alpha-7}} \tau_{ir} \quad (16)$$

provided that  $4\alpha - 7 \neq 0$ . In the opposite case, i. e. for  $4\alpha - 3\beta - 7 > 0$  the viscous forces are dominant for all  $t \ll t_{ir}$ . In case of the spreading of a constant volume, i. e. the solution of the Cauchy problem (1), (3) the viscous forces are dominant for  $t \gg t_{ir}$  where  $t_{ir}$  is given by Eq. (16) setting  $\alpha = 0$  and using  $\eta_f$  given by Eq. (7).

Consider the spreading of a constant volume and the spreading of a constant flux, i. e.  $\alpha = 1$ . The flow parameters, i. e.  $v_0$  and  $q$ , are chosen such that the transition time (Eq. (15))  $\tau_{ir}$  is equal to 1s for both cases. Setting  $t_0 = \tau_{ir}$  in Eq. (5) and shifting the time  $t \rightarrow t + t^*$ ,  $t^* = \max_{\beta \in [0, 3\alpha+1]} \{t_{ir}(\alpha, \beta)\} = t_{ir}(\alpha, 0) = \tau_{ir}$ , one obtains the initial data  $h_0(x) = h(x, t + t^*) \Big|_{t=0} = h(x, t^*)$  where  $h$  is either the solution of Eq. (1) with conditions (8) and (9) for  $\alpha = 1$  or the solution of Eq. (1) with the Cauchy-data given by Eq. (3). The initial shape  $h_0(x)$  is used to determine the initial conditions for the CORFLOW simulations. The comparison of the evolution of the interfaces  $x_f^+(t + t^*) - x_f^+(t^*)$  for the spreading of a constant mass flux and the spreading of a constant fluid volume for various values of  $\beta$  with the CORFLOW results are shown in Fig. 1 and Fig. 2, respectively.

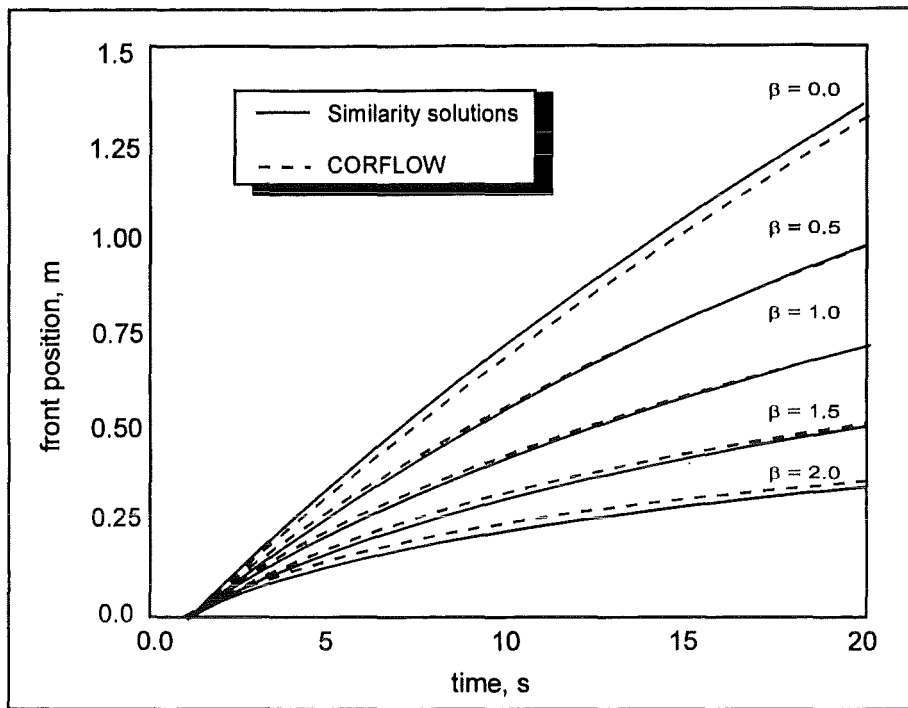


Fig. 1: Spreading of a constant volume flux

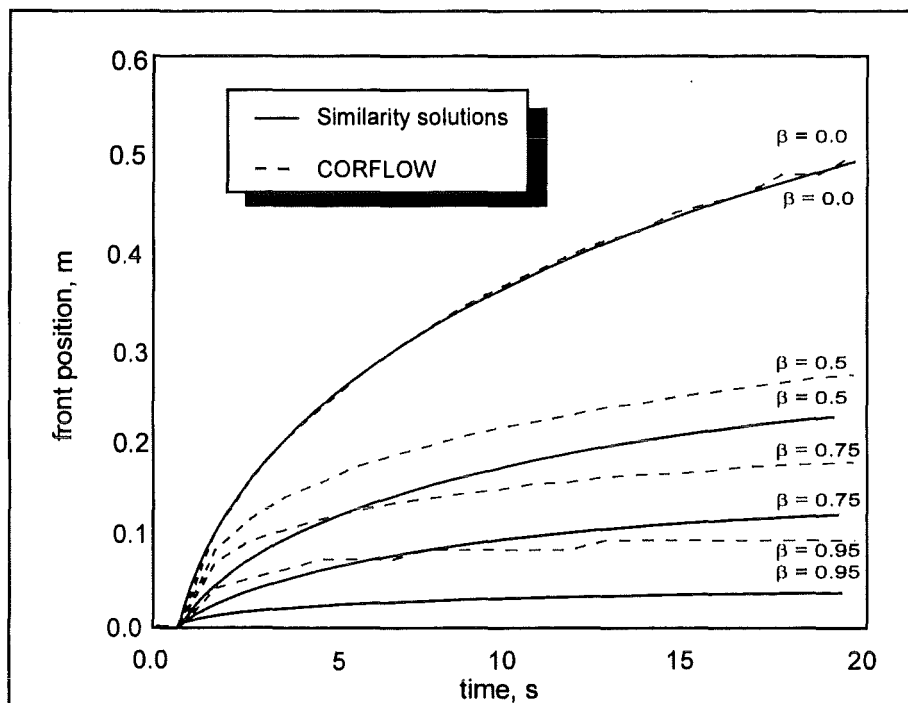


Fig. 2: Spreading of a constant fluid volume

The CORFLOW results are in good agreement with the theoretical predictions for the spreading of a constant flux with increasing viscosity represented by  $0 \leq \beta \leq 2$ , whereas, the agreement in the case of the spreading of a constant volume can be stated to be good only for  $0 \leq \beta < 0.5$ . For faster viscosity increase, i. e. for  $0.5 \leq \beta < 1$  CORFLOW overpredicts the front propagation considerably.

#### 4. Analysis of the oxidic KATS experiments

In the framework of large-scale KATS experiments (FZK, Germany) the non-isothermal spreading of metallic and oxidic melts on ceramic or concrete surfaces under various conditions are studied, e. g. melt overheat and melt release rates. The metallic and oxidic components of the melt are generated by the thermite reaction. The oxidic melt is composed of about 85 weight %  $\text{Al}_2\text{O}_3$ , 10 weight %  $\text{SiO}_2$  and about 5 weight %  $\text{FeO}$ . For the above melt mixture there is only a limited data base of material properties available. Using an estimated phase diagram, the Stedman correlation [13] was applied to evaluate the viscosity within the solidus-liquidus range. Above the liquidus temperature the experimental data of Elyutin et al. [14] were used [15]. An experimental program to measure the viscosity of the oxidic KATS melts below the liquidus temperature is under way.

The KATS experiments can be classified in accordance with the melt release conditions. In KATS7 [15] and KATS14 [16] the melt was not collected but it was poured into a cavity. As soon as the cavity was filled, the melt began to spread across the channel with flow rates defined by the diameter of the pouring nozzle. In this way an almost constant volumetric flux was achieved which lasted 12 s in the KATS7 test and 37 s in the KATS14 test. The melt front propagation ended at 49 s in the KATS7 and at 57.6 s in the KATS14 tests.

In the KATS5 [17] and KATS12 [18] experiments, on the other hand, the melts were gathered in a container before spreading into the channel was initiated by opening a gate in the container. Consequently, a linear decrease of the volumetric flow rate in time was obtained. The outflow of the oxidic melt from the container was completed after 3.7 s and 10.4 s in the KATS5 and KATS12 tests, respectively. The stop of the melt front was detected at 15 s in the KATS5 and 40 s in the KATS12 experiment. This class of experiments is suitable for comparison with the results obtained for the isothermal spreading given in Eq. (6) in order to see the effects of the melt cooling on the melt front propagation. According to the asymptotic

property (Eq. 4) this can be done for times which are larger than the outflow time from the container (Fig. 3).

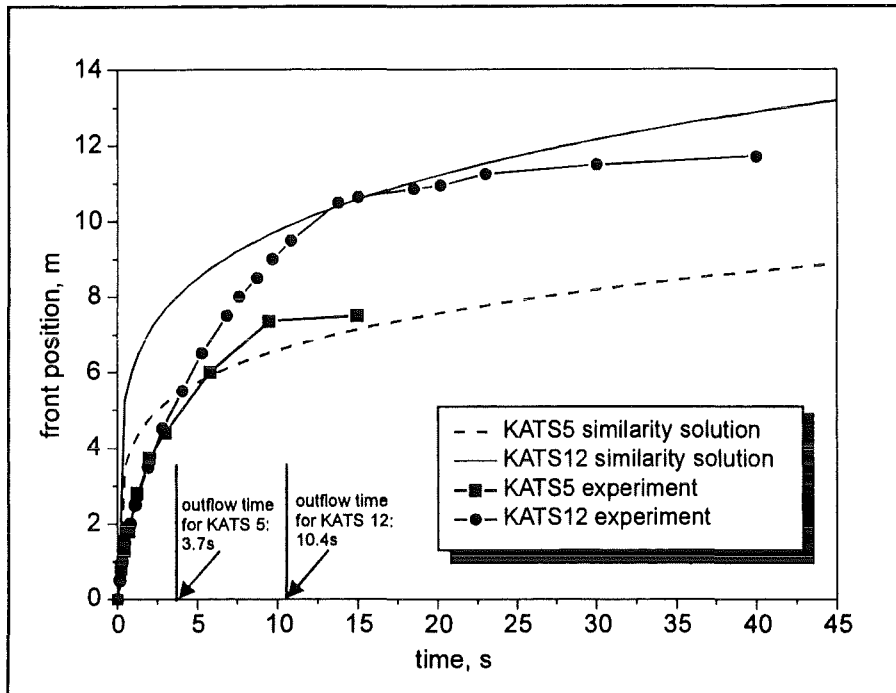


Fig. 3: Comparison of the front propagation in KATS5 and KATS12 with the self-similar solution for isothermal spreading of a constant volume

In both experiments the final front position is located in the neighbourhood of the isothermal curve. Due to the fairly large Péclet number for the oxidic melt under consideration, the spreading melt develops only a thin thermal boundary layer at the cooled boundaries. Consequently, the influence of this thin crust on the front propagation is weak until the time at which the gravity force is balanced by the strength of the developing crust.

#### 4.1 CORFLOW results

##### 4.1.1 Melt front progression

One can expect that the discrete phase transition model together with the variable viscosity approach used in the CORFLOW code will predict a stop of the melt front if almost all nodes at the free boundary reach the temperature at which the value of the viscosity becomes large and if the floating crust is connected to the basemat at the melt front. Because there is no crust failure criterion in CORFLOW, the results can depend strongly on the grid used for

simulations. The sensitivity on the grid size will generally depend on the viscosity behaviour as a function of the temperature and the initial condition of the melt release. In Fig. 4 the CORFLOW results using a fine grid and a coarse grid with double mesh size along the channel and triple mesh size in the vertical direction for the KATS5 experiment are shown as well as the experimental findings.

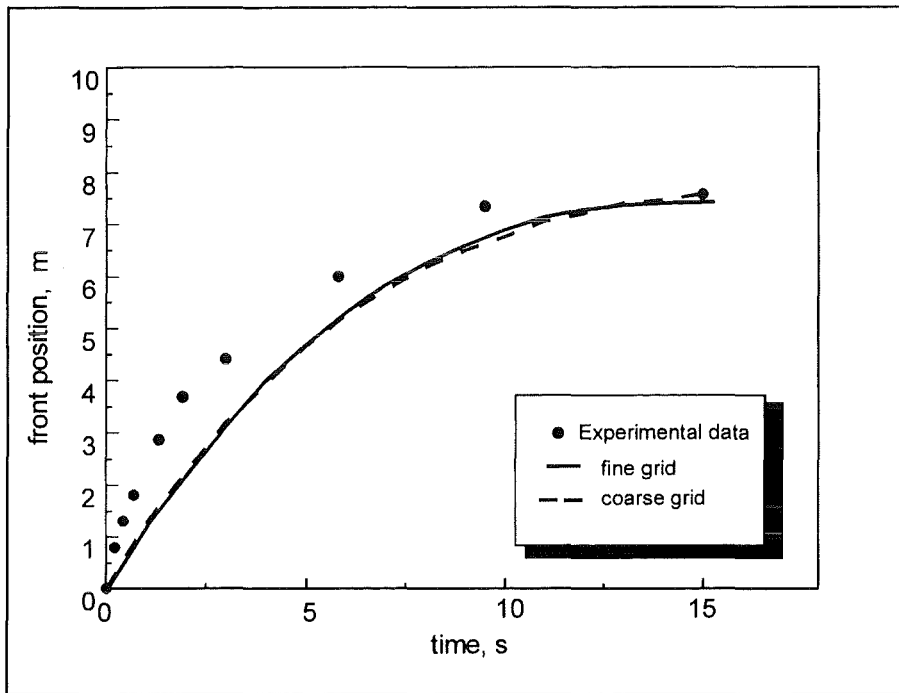


Fig. 4: Melt front progression for KATS5

Both CORFLOW results underpredict the speed of the melt front considerably during the melt release phase. The time of the end of the front propagation and the final front position agree well with the measurements in both simulations.

The simulation of the KATS12 experiment was performed using a coarser grid  $((\Delta x, \Delta z) = (0.1\text{ m}, 0.025\text{ m}))$ . The calculated front positions as a function of time are compared to the measured data in the following figure (Fig. 5)

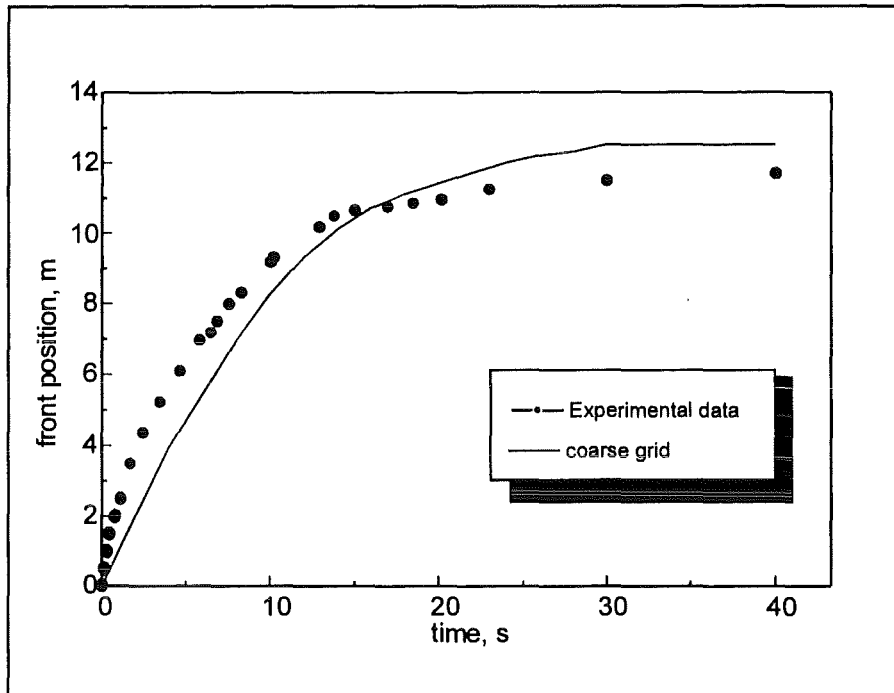


Fig. 5: Melt front progression for KATS12

As for the KATS5 experiment an underprediction of the melt front progression in the first stage of the spreading is predicted while the final front position agrees very well with the experimental one.

The results of the CORFLOW analysis of the second class of KATS experiments (experiments with an almost constant mass flux) the KATS7 and the KATS14 are shown in Fig. 6 and Fig. 7, respectively. The calculated evolution of the melt front during the melt release phase for the KATS7 agrees very well with the measured curve, in contrast to the previous cases. The time at which the melt front stops is predicted to be much shorter than detected in the experiment: 23 s for the fine grid and 27 s for the coarse grid calculation, whereas, it was measured to stop at 50 s in the experiment (Fig. 6). The discrepancies between the CORFLOW predictions and the measured front progression in the KATS14 experiment (Fig. 7) during the melt release phase might be due to the increase of the volumetric flux caused by an increase of the diameter of the pouring nozzle due to ablation. Both simulation underpredict the final front position. The stop of the melt front is predicted at 60 s for the fine grid and at 48 s for the coarse grid calculation. In the experiment the end of the melt front progression was detected after 58 s.

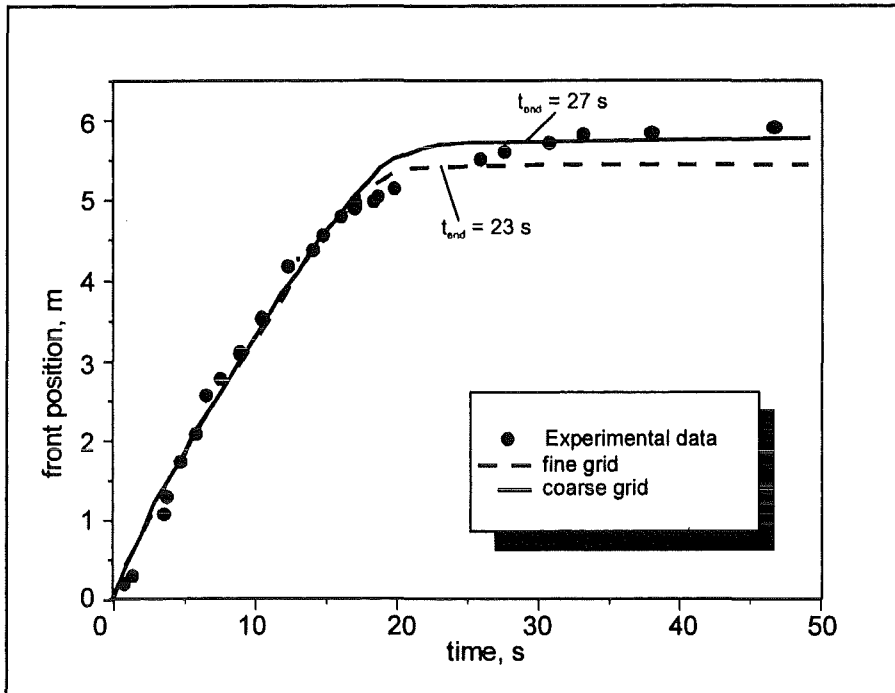


Fig. 6: Melt front progression for KATS7

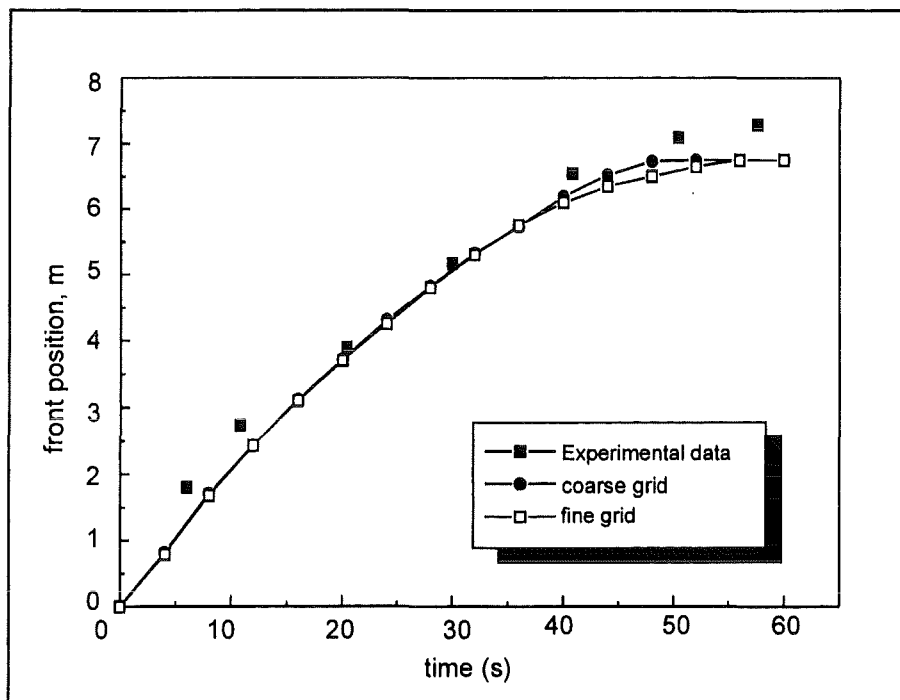


Fig. 7: Melt front progression for KATS14

#### 4.1.2 Temperature and velocity profiles for KATS5 experiment

The following figures (Fig. 8 - 9) show the time evolution of the thermal boundary layer in the vicinity of the melt front as predicted for the KATS5 experiment by CORFLOW. The temperature profiles are given as a function of the melt height. The mesh size in the vertical direction used in the fine grid calculation was chosen to be  $1 \cdot 10^{-3}$  m. The initial melt temperature was 2393 K. The liquidus temperature and the temperature at which the viscosity becomes infinite was estimated to be 2198 K and 2050 K, respectively [15]. The CORFLOW results show qualitatively reasonable resolution of the temperature field. While the melt continues to spread, the interface temperatures decrease and the thickness of the thermal boundary layers increases. The central temperature of the melt decreases only slowly and is still at about 2300 K far behind the front and at about 2180 K near the melt front after the end of the melt front propagation at 16 s. The comparison with the temperature profiles obtained by the coarse grid (triple mesh size in the vertical direction) (Fig. 8 - 9) shows the necessity of using a sufficiently refined grid in order to obtain a reasonable resolution of the thermal boundaries.

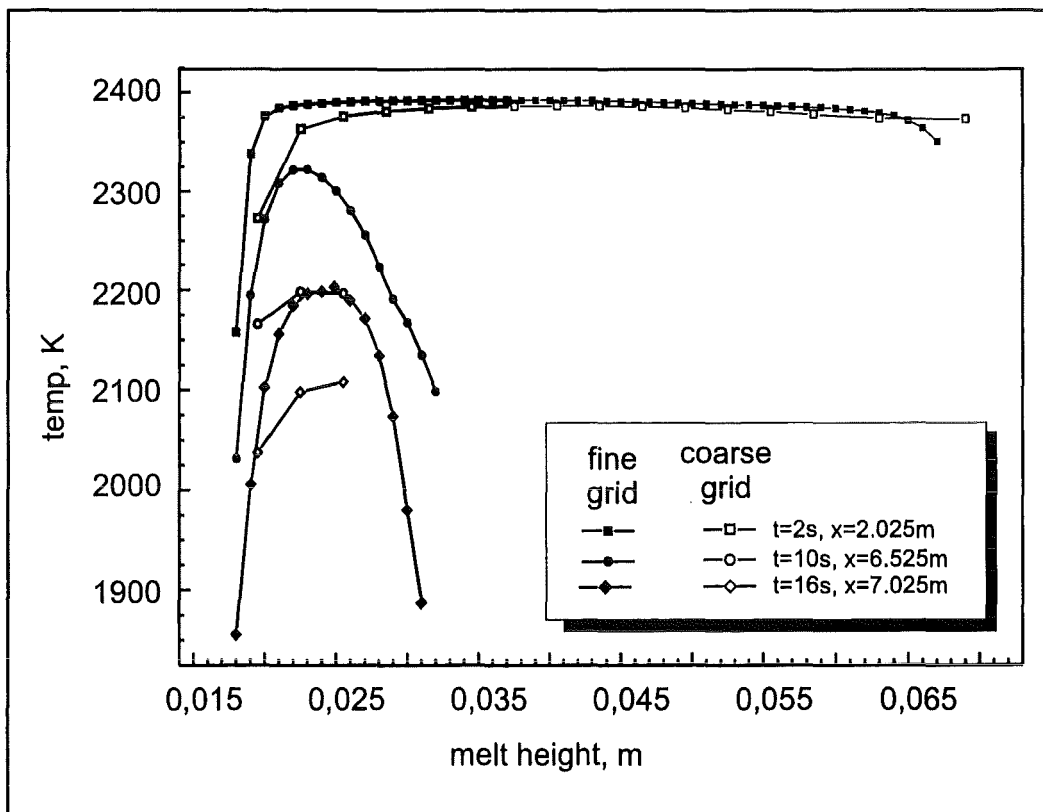


Fig. 8: Melt temperature as a function of the melt height near the melt front

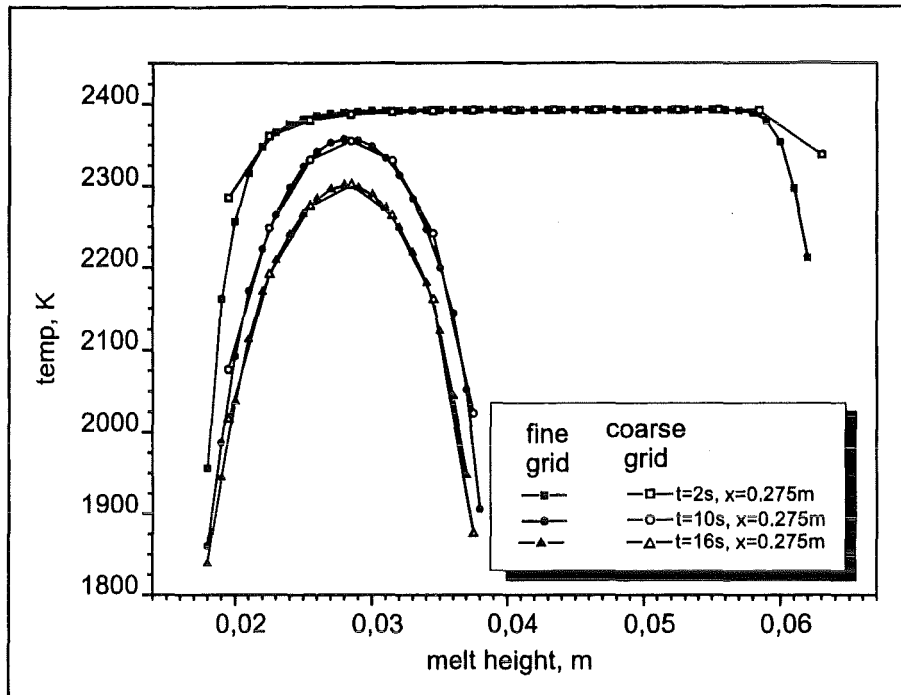


Fig. 9: Melt temperature as a function of the melt height far behind the melt front ( $x = 0.275 \text{ m}$ )

The profiles of the axial velocity corresponding to the locations and times given in Fig. 8 are depicted in the following figure (Fig. 10).

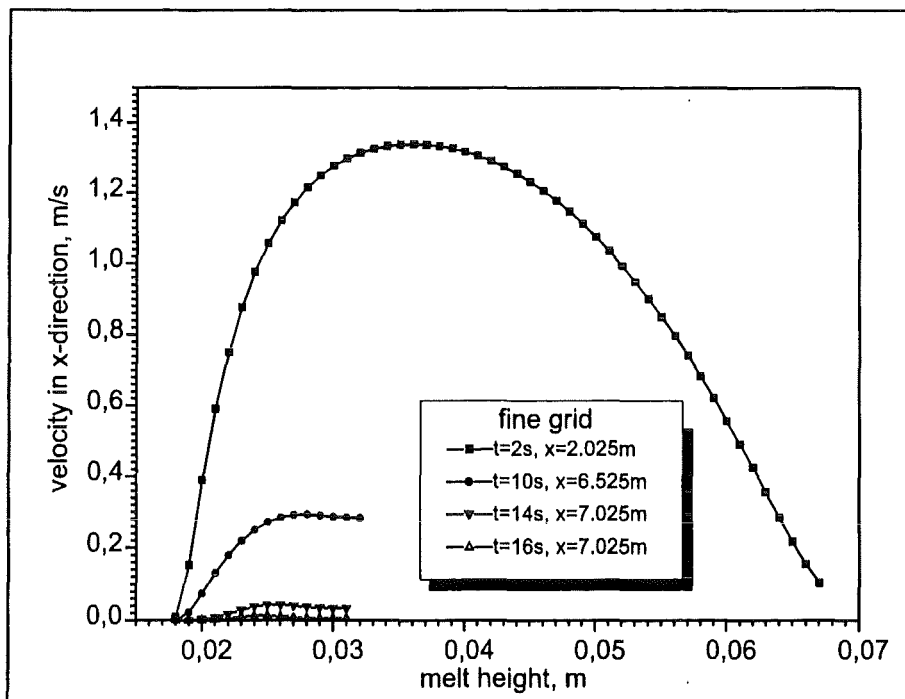


Fig. 10: Axial velocity as a function of the melt height near the melt front

The numerical procedure in CORFLOW does not contain a condition which ensures the continuity of the tangential component of the stress at the free surface. Therefore, it cannot be expected that CORFLOW will generally provide correct velocity profiles. It is obvious that the shear stress free condition is fulfilled if the temperature at the free surface reaches the temperature at which the viscosity becomes very large and a floating crust is built (Fig. 8 and Fig. 10).

#### 4.1.3 Energy losses

While the calculated total energy losses agree very well in both simulations, the energy partition depends strongly on the mesh size (Fig. 11, Fig. 12)

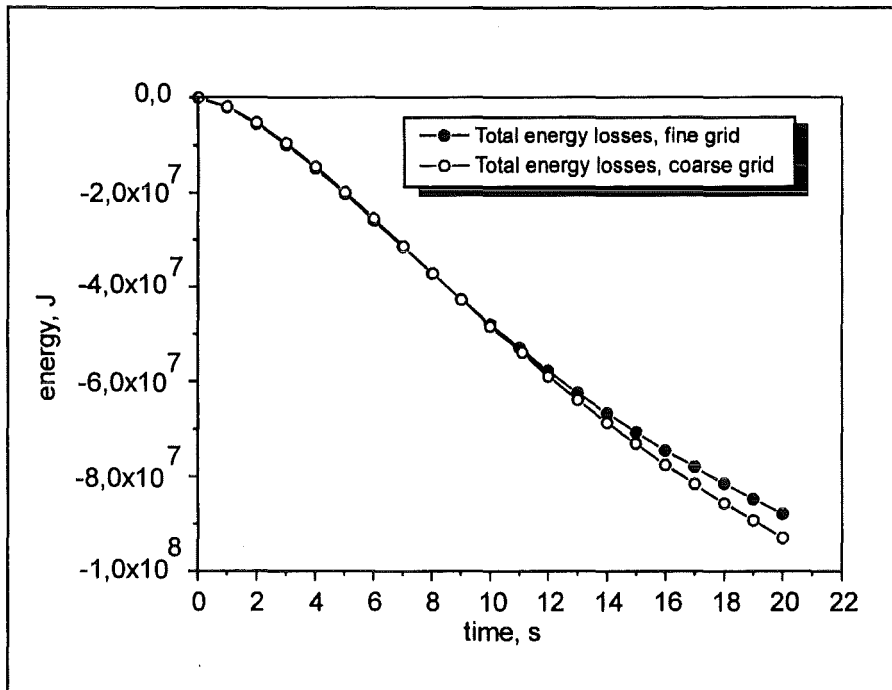


Fig. 11: Total energy losses for KATS5

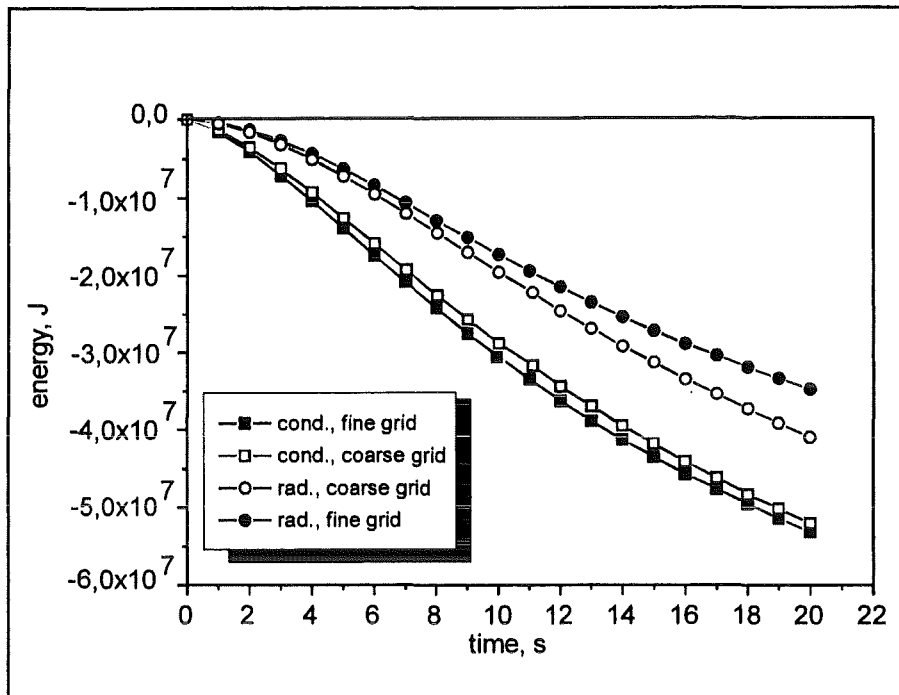


Fig. 12: Energy partition for KATS5

In all coarse grid calculations a decrease of the heat losses into the basemat by heat conduction and an increase of heat losses from the free surface by radiation is observed.

The following figures (Fig. 13 and Fig. 14) show the partition of the energy losses predicted by CORFLOW for the second class of the KATS experiments. The long release time of a hot melt leads to an increase of radiation losses. For the KATS14 experiment with a longest melt release phase (37 s) the losses due to radiation are predicted to be higher than those by diffusion into the basemat in both simulations.

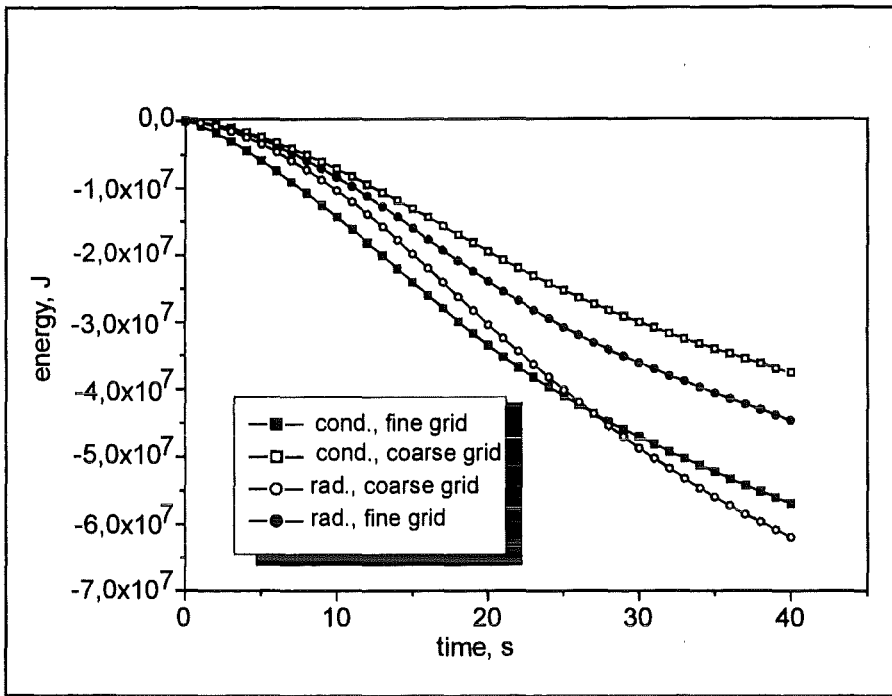


Fig. 13: Energy partition for KATS7

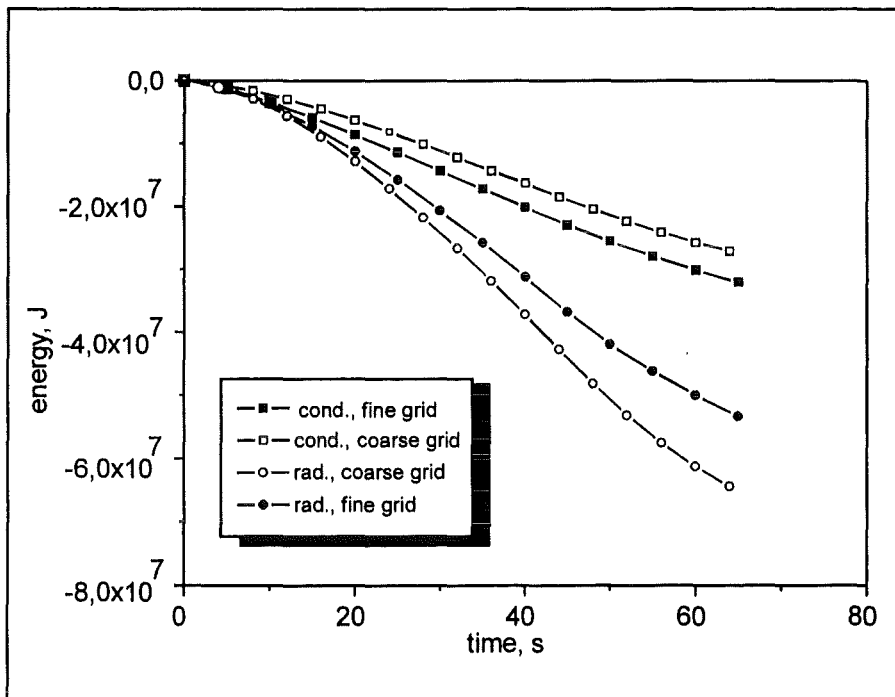


Fig. 14: Energy partition for KATS14

Even though the progression of the front and the final position of the front calculated for the oxidic KATS experiments are insensitive to the mesh size, i. e. to the resolution of the thermal boundaries and the partition of the energy losses, caution must be exercised if a coarse grid is used.

A comparison of the shape of the solidified melt found in the KATS14 oxidic experiment with the shapes predicted by CORFLOW using a fine and a coarse grid is shown in Fig. 15. The much greater melt height in the experiment is caused by the porous structure of the melt. The process of porous solidification, observed in all oxidic spreading experiment on ceramic (inert) substrate, is not well understood and far from being modelled. However, the height of the melt and the porous structure of the melt are of great importance for the coolability of the spreaded melt.

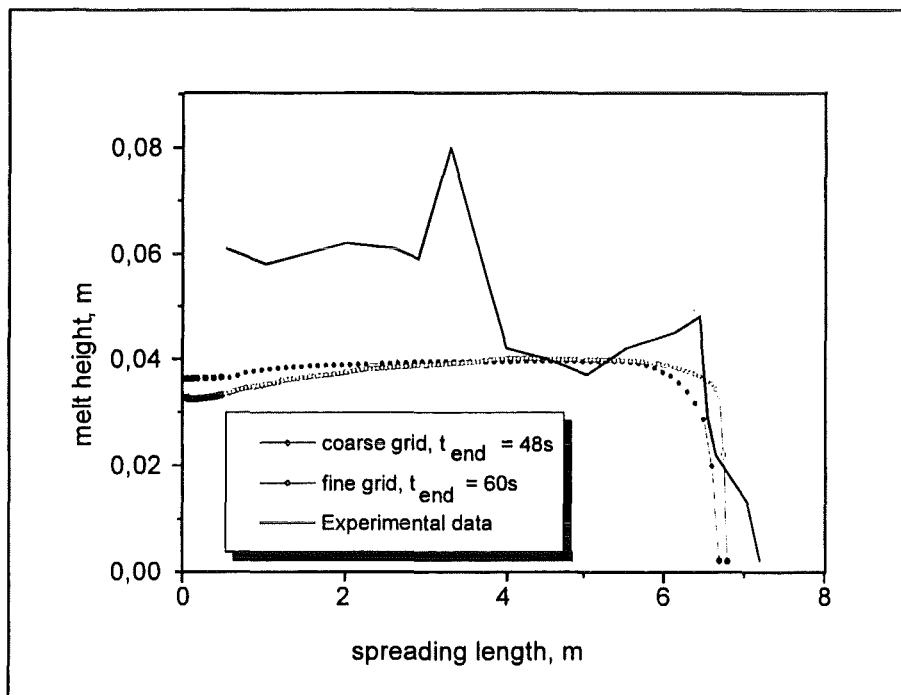


Fig. 15: Shape of the solidified melt (KATS14)

## 5. Conclusions

After the numerical deficiencies in the treatment of non-isothermal flows with increasing viscosity have been eliminated, there is a need for validation of the achieved modifications. For this purpose the self-similar solutions for spreading with variable viscosity are used. The CORFLOW results are in good agreement with the theoretical predictions for the spreading of a constant flux for a weak as well as for a strong increase of the viscosity with time. The agreement in the case of the spreading of a constant volume can be stated to be good only for a slow increase of the viscosity as a function of time. For faster viscosity increase CORFLOW overpredicts the front progression considerably.

Some of the KATS experiments (KATS5, KATS12) are suitable for comparison with the self-similar solutions for the isothermal spreading of a constant fluid volume in order to see the effects of the melt cooling on the front progression. In both experiments the final front position is located in the neighbourhood of the isothermal curve. Due to the fairly large Péclet number for the oxidic melt under consideration, the spreading melt develops only a thin thermal boundary layer at the cooled boundaries. Consequently, the influence of this thin crust on the front propagation is weak until the time at which the buoyancy force is balanced by the strength of the developing crust.

The variable viscosity used in CORFLOW seems to be adequate for simulations of the oxidic KATS experiments concerning the predictions of the final front position. The CORFLOW code will predict a stop of the melt front if almost all nodes at the free boundary reach the temperature at which the value of the viscosity becomes large and if the floating crust is connected to the basemat at the melt front. Because there is no crust failure criterion in CORFLOW, the results can depend strongly on the grid used for simulations. The sensitivity on the grid will generally depend on the viscosity behaviour as a function of the temperature and the initial condition of the melt release.

Even though the progression of the front and the final position of the front calculated for the oxidic KATS experiments are insensitive to the mesh size, i. e. to the resolution of the thermal boundaries and the partition of the energy losses, caution must be exercised if a coarse grid is used. Pronounced discrepancies are observed with respect to other details of the experimental findings such as the velocity of the melt front during the melt release and the time of the end of the front progression. The numerical procedure in CORFLOW does not contain a condition which ensures the continuity of the tangential component of the stress at the free surface.

Therefore, it cannot be expected that CORFLOW will generally provide correct velocity profiles.

When compared with the experimental database, overall, the CORFLOW code agrees well with some experimental data, and there are pronounced discrepancies with other experimental results. Discrepancy with experimental data may well be due to experimental nuances as much as poor models in the code, but, on the other hand, agreement with some experimental data should not be interpreted as justifying the underlying physical processes in the code (the data itself may not be fully qualified, and the agreement might have been obtained because of a fortuitous choice of input parameters). Therefore, additional validation is needed in order to reach a status in which one can rely on CORFLOW predictions of the spreading of the ex-vessel melt in a postulated meltdown accident. In addition, a sufficiently qualified data base of material properties for the ex-vessel core melts is required.

## References

- [1] Zel'dovich, Ya. B.; Kompaneets, A. S.: Collection Commemorating the 70<sup>th</sup> Anniversary of A. F. Joffe, *Izv. Akad. Nauk. SSR* (1950).
- [2] Sakimoto, S. E. H.; Zuber, M. T.: *J. Fluid Mech.* 301, 65 (1995).
- [3] Huppert, H. E.: *J. Fluid Mech.* 121, 43 (1982).
- [4] Foit, J. J.: FZKA-Report 6006, Forschungszentrum Karlsruhe (1997).
- [5] Bercovici, D.: *Geophys. Res. Lett.* 21, 1177 (1994).
- [6] Griffiths, R. W.; Fink, J. H.: *J. Fluid Mech.* 252, 667 (1993).
- [7] Stasiuk, M. V. et al.: *Geology* 21, 335 (1993).
- [8] Wittmaack, R.: *Nuclear Technology* 119, 158 (1997).
- [9] Buckmeister, J.: *J. Fluid Mech.* 81, 735 (1977).
- [10] Friedman, A.: *Variational Principles and Free Boundary Problems*, Robert E. Krieger Publishing Company, Malabar, Florida, 589 (1988).
- [11] Friedman, A.; Kamin, S.: *Trans. Amer. Math. Soc.* 262, No. 2, 551 (1980).
- [12] Foit, J. J.: In preparation.
- [13] Stedman, S. J. et al.: *J. Material Sci.* 25, 1833 (1990).
- [14] Elyutin, V. P. et al.: *Russian Journal of Physical Chemistry* 43, 3 (1969).
- [15] Fieg, G. et al.: FZKA-Report 6605, Forschungszentrum Karlsruhe (1997).
- [16] Fieg, G. et al.: Private communication.
- [17] Fieg, G. et al.: FZKA-Report 5920, Forschungszentrum Karlsruhe (1997).
- [18] Fieg, G. et al.: Private communication